Influence of structural properties on the activity of WO_3 catalysts for visible light photocatalytic ozonation

A. Rey[1]*, E. Mena[1], A.M. Chávez[1], F.J. Beltrán[1], F. Medina[2]

[1]Departamento de Ingeniería Química y Química Física, Universidad de Extremadura, Av. Elvas s/n, 06006 Badajoz (Spain)

[2]Department d'Enginyeria Quimica, Universitat Rovira i Virgili, Av. Països Catalans 26, 43007 Tarragona (Spain)

Abstract

This work is focused on the use of WO_3 catalysts with different structural properties for photocatalytic ozonation using visible light as radiation source. WO_3 catalysts were prepared by thermodecomposition of tungstite ($H_2O{\cdot}WO_3$) at 300-450ºC and different calcination time. Photocatalysts were characterized by means of TGA-DTA, XRD, N_2 adsorption-desorption isotherms, pH_{PZC}, XPS and DR-UV-Vis spectroscopy. Photocatalytic ozonation under visible light radiation with the catalyst calcined 5 min at 450ºC gave place to complete removal of ibuprofen in less than 20 min with 87% TOC removal at 120 min. This catalyst gave place to a complete removal of a mixture of ten emerging contaminants in a municipal wastewater in less than 60 min with 40% mineralization at 120 min. The highest catalytic activity of this material is due to the formation of monoclinic structure of WO_3.

Keywords

Photocatalytic ozonation, tungsten trioxide, crystalline structure, ozone, visible light

1. Introduction

The development of efficient water treatment technologies to remove organic pollutants such as solvents, dyes, pesticides, phenolic compounds or pharmaceuticals and personal care products, among others, is an important issue worldwide. In general, these pollutants are persistent, toxic and/or recalcitrant to conventional wastewater treatments and have shown to be a potential risk to human health and to the environment. Therefore, they must be removed in order to prevent their discharge and, of course, to fulfil the required limits of an increasingly stringent legislation.

Among the alternative technologies, the combination of ozone and heterogeneous photocatalysis with a semiconductor, i.e. photocatalytic ozonation, has demonstrated to efficiently remove organic compounds that are degraded little or slowly by photocatalysis or ozonation alone. The improvement of the combined process is mainly related to the formation of higher concentration of oxidizing species such as hydroxyl radicals compared to the single treatments (Agustina et al., 2005; Augugliaro et al., 2006). Usually, this treatment has been applied by using TiO_2 as photocatalyst and UV irradiation. However, from an environmental and economic point of view, the use of solar light is a need for the practical deployment of photocatalytic technologies. In this sense, TiO_2 presents some limitations since it only uses around 5% of solar radiation in the UV range in spite of being the archetypical photocatalyst due to its relatively high efficiency, low cost and availability (Hernández-Alonso et al., 2009).

Different research efforts have been carried out to overcome this limitation mainly focusing on the development of doped or modified TiO_2 or on the use of different semiconductors such as CdS, WO_3, SnO_2 or ZnO (Hernández-Alonso et al., 2009; Malato et al., 2009). Among them, bare tungsten trioxide WO_3 has been considered unsuitable for efficient photocatalytic oxidation due to its conduction band level respect to the reduction band level of O_2, whereas it has demonstrated an efficient behavior in the presence of O_3 (Nishimoto et al., 2010). WO_3 is a wide-band-gap semiconductor (2.6-3.0 eV) that can be excited with radiation corresponding to the visible region of the electromagnetic spectrum (Abe et al., 2008; González-Borrero et al., 2010). This fact together with its relatively low cost, no toxicity and availability make WO_3 an attractive alternative to TiO_2 for the photocatalytic ozonation processes under visible or solar light radiation.

The use of WO_3 in the photocatalytic ozonation process has been limited to commercial monoclinic WO_3 and phenol as target compound (Nishimoto et al., 2010; Mano et al., 2011). Thus, this work focuses on the study of WO_3 photocatalysts with different structural properties for the photocatalytic ozonation of a model compound using visible light radiation. Ibuprofen (IBP), a nonsteroidal anti-inflammatory drug, has been selected as target contaminant which is included in the family of emerging contaminants (ECs) frequently detected in wastewater and different aquatic environments (Barceló and Petrovic, 2008; Santos et al., 2009). In addition, a more realistic application of photocatalytic ozonation with WO_3 catalysts has been studied in a mixture of 10 ECs spiked municipal wastewater treatment plant (MWWTP) effluent using the entire simulated solar radiation spectrum.

2. Experimental section

2.1. Catalysts preparation

Photocatalysts were prepared by thermodecomposition of commercial H_2WO_4 (99%, Sigma-Aldrich) yellow powder precursor. The sample was calcined in air atmosphere in a muffle furnace at different temperatures (300 and 450ºC) for 1 to 30 min in order to obtain different H_2WO_4/WO_3 crystalline structures according to method reported by Cao et al. (Cao et al., 2012). The thermodecomposition reaction proceeds through water loss of the tungstite structure of H_2WO_4 ($H_2O{\cdot}WO_3$) and subsequent crystallization as cubic WO_3. Then, at higher temperature cubic WO_3 can be transformed into the monoclinic WO_3 crystalline phase (Guery et al., 1997). This process is summarized in eq. (1). **Table 1** shows the nomenclature of the catalysts and heat-treatment conditions together with some characterization results.

$$H_2WO_4(H_2O{\cdot}WO_3)_{tungstite} \xrightarrow{\Delta T,t} WO_{3,cubic} + H_2O$$
$$WO_{3,cubic} \xrightarrow{\Delta T,t} WO_{3,monoclinic} \quad (1)$$

2.2. Characterization

Thermal gravimetry and differential temperature analysis (TG-DTA) was performed with a SETSYS Evolution-16 apparatus (Setaram) using the following conditions: sample loading 20 mg, air flow 50 cm^3 min^{-1} at a heating rate of 5 ºC min^{-1} from room temperature to 600 ºC.

The crystalline phases present in the photocatalysts were inferred from their X-ray diffraction (XRD) patterns recorded using a powder Bruker D8 Advance XRD diffractometer with a Cu Kα radiation (λ=0.1541 nm). The data were collected from 2θ=10° to 70° at a scan rate of 0.02 s^{-1} and 1 s per point. Crystalline composition semi-quantitative analysis of the samples was performed on multi-phase patterns by the Reference Intensity Ratio (RIR) method using reference diffraction patterns by means of EVA v.14 software (Bruker-AXS). Due to the overlapping of the main characteristic peaks of the cubic and monoclinic WO_3 patterns, the analyses for the catalysts with monoclinic contribution were performed using a calculated value of RIR for the 2θ=28.6º diffraction peak corresponding to the (112) reflection plane.

BET surface area and pore volume of the photocatalysts were determined from their nitrogen adsorption–desorption isotherms obtained at -196ºC using an Autosorb 1 apparatus (Quantachrome). Prior to analysis the samples were outgassed at 150°C for 24 h under high vacuum (<10^{-4} Pa).

The point of zero charge (pH_{PZC}) of each sample was estimated using the mass titration method proposed by Subramanian et al. (Subramanian et al., 1988). Suspensions of the solid in deionized water at 5% (w/w) were prepared and the pH measured after 24 h of stirring.

X-ray photoelectron spectra (XPS) were obtained with a Kα Thermo Scientific apparatus with an Al Kα (hν=1486.68 eV) X-ray source using a voltage of 12 kV under vacuum ($2x10^{-7}$ mbar). Due to the lack of C 1s signal, binding energies were calibrated relative to the O1s peak of stoichiometric WO_3 at 530.2 eV (Senthil and Yong, 2007; Pang et al., 2013).

Diffuse reflectance UV-Vis spectroscopy (DR-UV-Vis) measurements, useful in the determination of the semiconductor band gap, were performed with an UV-Vis-NIR Cary 5000 spectrophotometer (Varian-Agilent Technologies) equipped with an integrating sphere device.

2.3. Catalytic activity measurements

Ibuprofen sodium salt (IBP), was used as target compound to test the catalytic activity of the synthesized materials. Photocatalytic experiments were carried out in semi-batch mode in a laboratory-scale system consisting of a 0.5 L glass-made spherical reactor, provided with a gas inlet, a gas outlet and a liquid sampling port. The reactor was placed in the chamber of a commercial solar simulator (Suntest CPS, Atlas) provided with a 1500 W air-cooled Xe arc lamp with emission restricted to visible light of wavelengths over 390 nm because of the presence of quartz, glass and polyester cut-off filters. The irradiation intensity was kept at 550 W m^{-2} and the temperature of the system was maintained between 25 and 35°C throughout the experiments. If required, a laboratory ozone generator (Anseros Ozomat Com AD-02) was used to produce a gaseous ozone-oxygen stream that was fed to the reactor. In that case, the ozone concentration was recorded on an Anseros Ozomat GM-6000Pro gas analyzer.

In a typical photocatalytic ozonation experiment, the reactor was first loaded with 0.5 L of an aqueous solution containing 10 mg L^{-1} of IBP initial concentration at pH_0=6.5 (not buffered). Then, 0.125 g of the catalyst were added and the suspension was stirred in the darkness for 30 min. After this dark stage, the lamp was switched on and, simultaneously, a mixture of ozone-oxygen (10 mg L^{-1} ozone concentration) was fed to the reactor at a flow rate of 20 L h^{-1}. The irradiation time for each experiment was 2 h. Samples were withdrawn from the reactor at intervals and filtered through a 0.2 μm PET membrane to remove the photocatalyst particles except for dissolved ozone analysis.

Experiments of adsorption (i.e., absence of radiation and ozone), photolysis (i.e., radiation in absence of catalysts and ozone), photocatalytic oxidation (i.e., radiation and catalyst in absence of ozone), ozonation (i.e., absence of radiation and catalyst), catalytic ozonation (i.e., absence of radiation) were also carried out for comparative analysis.

In addition, the effectiveness of the best photocatalytic system was tested in a more realistic application under complete simulated solar light radiation (wavelength from 300 nm). Ten emerging contaminants: acetaminophen (AAP), metoprolol (MTP),

caffeine (CAF), hydrochlorothiazide (HCT), antipyrine (ANT), sulfamethoxazole (SFM), carbamazepine (CAR), ketorolac (KET), diclofenac (DCF) and ibuprofen (IBP); frequently found in municipal wastewater effluents (MWW), were selected. They were added at initial concentration of 0.5 mgL^{-1} to a MWW taken from Badajoz MWWTP (Badajoz, Spain) designed for 225,000 inhabitants with an average inlet flow of 37,500 m^3 day^{-1}. Effluents were collected downstream of the MWWTP secondary biological treatment and filtered. The carbonate-bicarbonate content was eliminated by air stripping after acidifying the MWW. Then pH was restored and MWW was stored at -20ºC until use.

IBP concentration was analyzed by high-performance liquid chromatography HPLC-DAD (Hitachi, Elite LaChrom) using a Phenomenex C-18 column (5 µm, 150 mm long, 3 mm diameter) as stationary phase and 0.7 mL min^{-1} of acetonitrile-acidified water (0.1% H_3PO_4) as mobile phase (60-40 v/v, isocratic). Identification and quantification was carried out at 220 nm. ECs concentration in MWW matrix were analyzed by the same HPLC system with 0.2 mL min^{-1} of acetonitrile-acidified water (0.1% formic acid) as mobile phase with a gradient from 10% to 100% in acetonitrile in 40 min and 20 min re-equilibration time. Identification and quantification was carried out at the maximum wavelength of each compound. Total organic carbon (TOC) was measured using a Shimadzu TOC-V_{SCH} analyzer. Aqueous ozone was measured by following the indigo method using an UV-Visible spectrophotometer (Evolution 201, Thermospectronic) set at 600 nm (Bader and Hoigné, 1981). Ozone in the gas phase was continuously monitored by means of an Anseros Ozomat GM-6000Pro analyzer. Hydrogen peroxide concentration was determined photometrically by the cobalt/bicarbonate method, at 260 nm using a UV-Visible spectrophotometer (Evolution 201, Thermospectronic) (Masschelein et al., 1977).

3. Results and discussion

3.1. Characterization of the photocatalysts

Tungstite is a hydrous tungsten oxide, $H_2O{\cdot}WO_3$ that crystallizes in the orthorhombic system and can be thermally decomposed into different WO_3 structures. WO_3 consists of a three-dimensional array of corner sharing metal-oxygen octahedral in a chess-board type of array. The ideal structure is a ReO_3-type cubic form but this is easily distorted away since the relatively small tungsten atoms tend to be displaced from the centres of the octahedral. These displacements are temperature dependent and also influenced by the presence of impurities that make WO_3 adopts a variety of symmetry types: monoclinic, triclinic, orthorhombic and tetragonal. In addition, another two metastable structures of WO_3 have been obtained at low temperatures: hexagonal and pyrochlore (Tilley, 1995).

Thus, the thermal behaviour of the commercial tungstite precursor is mandatory to understand the crystallization of the different WO_3 structures. **Fig.1** shows the ATG-DTA profiles for the H_2WO_4 precursor. The evolution can be divided in 4 different regions. First of all, from ambient temperature to 150ºC, a small weight loss around 1%

is observed accompanied by an endothermic contribution which can be assigned to the evaporation of adsorbed H_2O. In region II, from 150 to 325ºC, a noticeable weight loss is obtained together with an endothermic peak at 225ºC which corresponds with the loss of coordinated H_2O from the tungstite structure to form cubic WO_3 (Guery et al., 1997; Cao et al., 2012). The cubic WO_3 structure is metastable and it can be stabilized by the presence of Na^+ impurities (Szilágyi et al., 2012). However, at this temperature, formation of different structures such as monoclinic WO_3 cannot be disregarded as it is expected from the absence of impurities in the commercial precursor used here. On the other hand, in the range 325-500ºC (region III), it can be observed a slight endothermic contribution around 371ºC followed by an exothermic peak with a maximum centred at 447ºC together with a slight weight loss around 0.2%. In this region, the complete transformation of cubic WO_3 into monoclinic WO_3 occurs (Guery et al., 1997; Cao et al., 2012). No significant changes are observed in region IV in the range 500-600ºC. From these results, the heat-treatment temperature of the precursor was set at 300 and 450ºC to obtain different crystalline phases composition of the catalysts. The time of the heat-treatment was relatively short (1-30 min) following the work of Cao et al., 2012. One catalyst was also heat-treated during 60 min for comparative purposes.

The structural characterization of the catalysts was performed by XRD as shown in **Fig.2** where XRD patterns of the tungstite $H_2O{\cdot}WO_3$ orthorhombic phase (JCPDS 018-1418), cubic WO_3 (JCPDS 41-0905) and monoclinic WO_3 (JCPDS 043-1035) have been plotted for comparison. It can be noticed that the main peaks in the diffraction pattern of the precursor, W-0, are attributable to the orthorhombic phase of tungstite, although a small shoulder around 24.2º can also indicate a low contribution of the cubic WO_3 phase. When the precursor is heat-treated at 300ºC the cubic structure of WO_3 is progressively formed as the time of calcination increases. Thus, for 1 min at 300ºC (W_{300}-1) it can be observed the coexistence of tungstite orthorhombic phase together with cubic WO_3, as the main peaks of tungstite at 16.5 and 25.6º decreased in favour of the increasing cubic diffraction peaks. The transformation of tungstite into cubic WO_3 has been completed in the W_{300}-3 catalyst, where the main tungstite diffraction peaks have completely disappeared and all the diffraction peaks are attributable to cubic crystalline structure. After that, an increase in the time of calcination at 300ºC provokes the formation of monoclinic WO_3 to some extent. This can be noticed by the presence of the contributions centred at 26.5 and 28.6º. These are characteristics of the monoclinic crystalline structure, together with the widening of the peaks at 23.9 and 34.0º that are affected by the overlapped cubic-monoclinic contributions with the formation of the triple peaks in monoclinic phase at these 2θ values corresponding to reflections from (001), (020) and (200) planes (Senthil and Yong, 2007). It is also noticeable that an increase of the calcination time from 5 to 60 min did not produce any significant change in the XRD patterns (W_{300}-5 and W_{300}-60) which is indicative of the stabilization of the cubic structure at this temperature. Finally, the temperature increase from 300 to 450ºC provoked the transformation of the cubic phase of WO_3 into monoclinic one to a greater extent according to previous TGA-DTA results. **Table 1** shows the semiquantitative analysis of crystalline phases in the catalysts.

Table 1 also summarizes the BET surface area values of the catalysts from N_2 adsorption-desorption isotherms. In general, small surface areas are obtained in this type of materials unless different strategies were used to this purpose. As can be observed, the surface areas undergo a slight increase (from c.a. 30 to 40 m^2g^{-1}) when the dehydration of tungstite occurs and cubic crystalline structure is formed. On the other hand, at higher calcination temperature, a decrease of the surface area is observed in the 450ºC catalysts, being higher as the time of the heat treatment increases.

The pH of the point of zero charge was also determined for the catalysts studied and these results are summarized in **Table 1**. The acidity of the surface can play a significant role in the behaviour of WO_3 based materials in wastewater treatments in adsorption processes of organic compounds and species with unpaired electrons (Tomova et al., 2012). It can be noticed a slight decrease in the value of pH_{PZC} together with the transformation of tungstite into WO_3 cubic structure so that the catalysts with this majority crystalline phase have a pH_{PZC} value around 4. On the other hand, an increase in the calcination temperature to up to 450ºC led to values of pH_{PZC} around 5 for W_{450}-5 and W_{450}-30 catalysts. The decrease of the surface acidity with increasing calcination temperature has been previously reported in monoclinic WO_3 (Kanan et al., 2002) and WO_3-ZrO_2 catalysts (Sun et al., 2000), and has been attributed to the creation of vacancies in the WO_3 structure from the extraction of lattice oxygen, which leads to a decrease in the number of Lewis acid sites (Kanan et al., 2002). In addition, a higher calcination temperature could also produce the dehydration/dehydroxilation of the WO_3 surface to some extent lowering the number of Brönsted acid sites (Kanan et al., 2002).

Surface characterization of the catalysts was performed by XPS to analyse the stoichiometry and chemical binding states of W. XPS spectra of W 4f region are depicted in **Fig.S1** of the supplementary information. In all cases, the spectra obtained showed a doublet with binding energies around 35.5 and 37.6 eV for W $4f_{7/2}$ and W $4f_{5/2}$, respectively, with the W $4f_{7/2}$-W$4f_{5/2}$ binding energy separation being 2.1 eV. The energy position of this doublet corresponds to the W^{6+} oxidation state in WO_3 (Senthil and Yong, 2007; Lee et al., 2012; Pang et al., 2013). On the other hand, XPS spectra of O 1s spectral region for all the catalysts are shown in **Fig.S2**. The main contribution at 530.2 eV has been assigned to oxygen in the WO_3 lattice (Azimirad et al., 2007; Senthil and Yong, 2007; Pang et al., 2013). Moreover, an additional contribution centred at 532.5 eV has been observed for W-0 and W_{300}-1 catalysts, which has been assigned to oxygen in water molecules bound in the tungstite structure ($H_2O{\cdot}WO_3$) or absorbed in the catalyst surface (Senthil and Yong, 2007). This is consistent with TGA-DTA and XRD results having these two catalysts more than 80% of tungstite in their structure.

The diffuse reflectance UV-Vis spectra of the photocatalysts (**Fig.3**) showed a higher optical absorbance in the visible region up to ca. 530 nm for tungstite composed catalysts (W-0 and W_{300}-1) whereas decreased to ca. 480 nm for cubic and monoclinic WO_3 composed catalysts (W_{300}-3, W_{300}-5, W_{450}-5, W_{450}-30). The optical energy band gap (E_g) was calculated by means of Tauc's expression in **Fig.S3** (supplementary

information), and results are summarized in **Table 1**. These values are approximate due to the need of extrapolation of the resulting curve as can be observed in **Fig.S3** for all the catalysts. The E_g value for tungstite H_2WO_4 (major component of W-0 and W_{300}-1) was found to be 2.42 eV which is increased up to 2.64 when the precursor is completely transformed into cubic WO_3 structure (in W_{300}-3 catalyst). Then, the E_g value was progressively increased up to 2.67 eV as monoclinic WO_3 was formed. These results are quite similar to previously reported values (González-Borrero et al., 2010; Cao et al., 2012).

3.2. Comparison of processes

The effectiveness of the photocatalysts in the use of visible light radiation combined with ozone was tested using IBP as target compound by cutting off all the wavelengths lower than 390 nm of the Xe lamp in the solar simulator. First, the performance of the combined process (photocatalytic ozonation) respect to the single treatments has been checked with all the catalysts. Results obtained with W_{450}-5 catalyst are depicted in **Fig.4** and **Fig.5,** being this catalyst representative of the behaviour of the most active ones. **Fig.4(A)** shows the time evolution of IBP dimensionless concentration upon the different treatments applied. First of all, the absence of IBP depletion due to direct photolysis with visible light radiation was confirmed which is consistent with the UV-Vis absorption spectrum of this compound (**Fig.S4** of supplementary information). On the other hand, IBP adsorption capacity of the W_{450}-5 catalyst at the conditions studied here was somewhat noticeable, reaching around 10% of IBP removal after 2 h contact time. The depletion rate of IBP is increased in photocatalytic oxidation reaching 25% of IBP removal after 2 h of treatment although it can be noticed the low efficiency of the process as a consequence of the high recombination rate in WO_3 materials used in the presence of oxygen (Nishimoto et al., 2010). When O_3 is present, all the treatments led to complete IBP removal in less than 1 h of reaction time (with conversion higher than 99%) regardless of the presence/absence of catalyst and/or radiation in contrast to O_3-free treatments. Although the evolution of IBP is quite similar for all the O_3-treatments, some slight differences can be observed in the depletion rate. Single ozonation and photolytic ozonation presented quite similar IBP depletion rate. On the other hand, the presence of the W_{450}-5 catalysts and ozone in dark conditions (catalytic ozonation) did not improve the degradation of IBP thus indicating that this catalyst does not possess any catalytic effect in ozone decomposition into reactive species such as hydroxyl radicals or even could produce an inefficient decomposition for IBP degradation. Photocatalytic ozonation gave place to the highest IBP depletion rate reaching complete IBP removal in 20 min compared to 40-50 min necessary for the other O_3 treatments.

On the other hand, it is known that the oxidation of IBP proceeds through different steps giving place to different intermediate compounds which are eventually transformed into CO_2 and H_2O (complete mineralization). Thus, the mineralization of IBP has been followed and presented in **Fig.4(B)** as normalized TOC concentration. As expected from previous IBP results, neither adsorption nor direct photolysis led to significant mineralization percentages. Photocatalytic oxidation also gave place to

negligible mineralization according to the IBP conversion reached, lower than 25%. Regarding the O_3-treatments, noticeable differences have been found depending on the presence/absence of O_3, radiation and/or photocatalyst. Single ozonation led to 25% of mineralization reached at 60 min and then stopped both as a consequence of the formation of some intermediate compounds that are refractory to ozone direct reaction (mainly short-chain organic acids) (Beltrán, 2004), and/or due to the absence of IBP in the reaction medium which eventually produces hydroxyl radicals through IBP-O_3 direct reaction as discussed below. Fairly similar results were observed during photolytic ozonation with visible light radiation. On the other hand, the presence of the catalyst combined with ozone in dark conditions (catalytic ozonation) did not improve the previous results. This process showed the poorest behavior of the O_3-treatments in terms of mineralization, with negligible TOC conversion during the reaction time, confirming the absence of any positive catalytic effect in the reaction. In fact, the low mineralization reached compared to ozone alone treatment is likely indicative of an inefficient consumption of O_3 in the catalyst surface in the darkness. These results are contrary to those found for the mineralization of phenol with a commercial WO_3 (monoclinic) catalyst (Nishimoto et al., 2010), which points out the importance of the target compound nature to play a key role in the interactions compound-catalyst surface during catalytic ozonation. On the contrary, photocatalytic ozonation showed the highest mineralization rate, leading to 87% mineralization in 120 min reaction time. These results also point out the synergism produced between ozone and visible light irradiated WO_3 since final TOC removal of the combined process is much higher than the sum of these values for the individual processes (87% in O_3/WO_3/Vis vs. 5% in O_2/WO_3/Vis and 25% in O_3), confirming also the ability of O_3 to capture the electrons on the WO_3 surface compared to O_2 (Nishimoto et al., 2010).

In addition, time profiles of dissolved ozone and hydrogen peroxide concentration during the treatments have been plotted in **Fig.5**. Regarding dissolved ozone, in **Fig.5(A)** it is seen that ozone accumulated in solution during the single ozonation experiment reaching a maximum concentration at about 60 min reaction time. Different profiles were observed in the other O_3-treatments in which ozone concentration increased in the first minutes of the experiment and then remained almost constant. The ozone concentration was always lower in catalytic ozonation than during single ozonation. This observation together with the low mineralization reached, is an additional evidence of an inefficient decomposition of O_3 on the catalyst surface in the darkness. On the other hand, in the photocatalytic ozonation process, the maximum concentration of dissolved ozone was noticeably lower, leading to a nearly steady concentration of about $1x10^{-5}$ M in contrast to $5x10^{-5}$ M during single ozonation. The lowest values of dissolved ozone together with the highest mineralization rate observed in this treatment suggest that O_3 has been consumed on the WO_3 catalyst surface through its reaction with electrons generated in the photocatalytic process, thus enhancing the production of oxidizing species such as hydroxyl radicals, as with TiO_2 catalysts (Agustina et al., 2005; Augugliaro et al., 2006; Mena et al., 2012).

On the other hand, hydrogen peroxide is commonly formed through direct ozone reactions (Rakowski and Cherneva, 1990; Mvula and von Sonntag, 2003; Leitzke and

von Sonntag, 2009). This has been experimentally confirmed in this work for IBP, as shown in **Fig.5(B)**. Thus, during single ozonation an increase in H_2O_2 concentration up to 45 min, when IBP was completely removed, can be observed. Then, H_2O_2 concentration remained almost constant until the end of the experiment. The concentration of H_2O_2 formed during catalytic and photolytic ozonation was somewhat lower. On the other hand, during photocatalytic ozonation the formation of H_2O_2 takes place at higher rate reaching a maximum concentration at about 20-30 min when IBP was completely removed. Then the consumption of H_2O_2 was faster and the concentration negligible at the end of the treatment. These results point out that H_2O_2 is being consumed through photocatalytic reactions probably acting as an electron acceptor in the WO_3 surface thus increasing the production of hydroxyl radicals and avoiding recombination to some extent, as also occurs with TiO_2 (Mena et al., 2012). Finally, the formation of H_2O_2 during photocatalytic oxidation was much lower than in ozone processes confirming the production of H_2O_2 mainly through direct IBP-O_3 reaction.

Therefore, compared to individual processes, photocatalytic ozonation treatment with WO_3 and visible-light radiation led to a faster IBP depletion with the highest mineralization rate due to the synergistic effect between O_3 and irradiated WO_3.

3.2.1. Simplified mechanistic approach of IBP photocatalytic ozonation

Direct ozone reactions in water follow second order kinetics and the kinetic regime can be established through the determination of the Hatta number according to (Beltran, 2004):

$$Ha = \frac{\sqrt{k_{IBP-O3} D_{O3} C_{IBP}}}{k_L} \quad (2)$$

Where D_{O3}=1.3x10^{-9} m^{2}s^{-1} is the ozone diffusivity in water (Johnson and Davis, 1996), and k_L=5x10^{-5} ms^{-1} is the individual liquid phase mass transfer coefficient for a bubbled stirred tank (Froment and Bishoff, 1979), being C_{IBP} the molar IBP concentration and k_{IBP-O3}=9.1 M^{-1}s^{-1} the direct reaction rate constant (Huber et al., 2005). The highest calculated value was 0.023 for the initial conditions thus confirming slow kinetic regime of ozone absorption. Thus the depletion rate of IBP through direct O_3 reaction is described as follows:

$$-\frac{dC_{IBP}}{dt}\Big)_{O_3} = \frac{1}{z} k_{IBP-O_3} C_{O_3} C_{IBP} \quad (3)$$

Where z=1 is the stoichiometric coefficient of the reaction in mol O_3/mol IBP and C_{O3} is the dissolved ozone concentration. The differential equation (3) was solved using the value of the kinetic constant and the experimental values of C_{O3} by means of 4th order Runge-Kutta. The results of simulated dimensionless C_{IBP} together with the

experimental values during single ozonation are depicted in **Fig.6**. It can be clearly noticed that the experimental rate of IBP depletion is higher than the expected results (simulated), thus indicating that additional reactions may develop and contribute to IBP removal. Indirect reactions due to O_3 decomposition are initiated through the following steps:

$$O_3 + OH^- \longrightarrow HO_2^- + O_2 \quad (4)$$

$$H_2O_2 \underset{}{\overset{pK=11.3}{\rightleftharpoons}} HO_2^- + H^+ \quad (5)$$

$$HO_2^- + O_3 \longrightarrow O_3^{\bullet -} + HO_2^{\bullet} \quad (6)$$

$$HO_2^{\bullet} \underset{}{\overset{pK=4.8}{\rightleftharpoons}} O_2^{\bullet -} + H^+ \quad (7)$$

$$O_2^{\bullet -} + O_3 \longrightarrow O_3^{\bullet -} \quad (8)$$

$$O_3^{\bullet -} + H^+ \longrightarrow [...] \longrightarrow HO^{\bullet} \quad (9)$$

These reactions lead to the formation of hydroxyl radicals ($HO^{\bullet}$) capable of oxidizing IBP in water. However, the pH of the reaction was from 6.5 to 4.5 and therefore, reaction (4) between O_3/OH^- seems not to play an important role on the IBP disappearance. In addition, the accumulation of H_2O_2 was observed during the single ozonation experiment at these pH (**Fig.5(B)**), thus indicating that the reaction (6) between O_3/ HO_2^- can be also disregarded. These evidences together with the evolution of mineralization whereas IBP is still present in the reaction medium during single ozonation lead to hypothesize the formation of ozonide radical through IBP-O_3 direct reaction, as it has been previously reported for phenol or diclofenac (Mvula and Sonntag, 2003; Buffle and von Gunten, 2006; Sein et al., 2008):

$$IBP + O_3 \longrightarrow INT + O_3^{\bullet -} \quad (10)$$

which immediately results in the formation of $HO^{\bullet}$ through reaction (9), being INT any intermediate organic compound.

With these considerations, the depletion rate of IBP through direct O_3 reaction taking into account the formation of $HO^{\bullet}$ during this reaction is described as follows:

$$\left(-\frac{dC_{IBP}}{dt}\right)_{O_3-HO\cdot} = k_{IBP-O_3} C_{O_3} C_{IBP} + k_{IBP-HO\cdot} C_{HO\cdot} C_{IBP} \quad (11)$$

$$\left(\frac{dC_{HO\cdot}}{dt}\right)_{IBP-O_3} = k_{IBP-O_3} C_{O_3} C_{IBP} - k_{IBP-HO\cdot} C_{HO\cdot} C_{IBP} \quad (12)$$

Where $k_{IBP\text{-}HO\cdot}$ is the rate constant between hydroxyl radical and IBP and $C_{HO\cdot}$ is the hydroxyl radical concentration. The differential equations (11) and (12) were simultaneously solved using the value of the kinetic constants and the experimental values of C_{O3} by means of 4th order Runge-Kutta ($k_{IBP\text{-}HO\cdot}$=7.4x10^9 M^{-1}s^{-1}, Huber et al. (2005)). These results are also depicted in **Fig.6**, where it can be observed that the experimental IBP depletion rate is still higher than the simulated values. This could be related to the accuracy of the rate constants used for the simulation and/or the development of additional IBP degradation routes. The confirmation of the different degradation ways needs extra experiments out of the scope of this work.

According to this and the previous findings, it can be postulated that photocatalytic ozonation of IBP with WO_3 catalyst takes place through reactions (13)-(20), where both O_3 and $HO^\bullet$ are responsible for IBP disappearance and photogenerated oxidizing species ($HO^\bullet$ and/or positive holes) are the main responsible for mineralization.

$$IBP + O_3 \longrightarrow [...] \longrightarrow INT + H_2O_2 + [HO^\bullet] \quad (13)$$

$$WO_3 \xrightarrow{h\nu} WO_3(e^-) + WO_3(h^+) \quad (14)$$

$$WO_3(e^-) + O_3 \longrightarrow [...] \longrightarrow HO^\bullet \quad (15)$$

$$WO_3(e^-) + H_2O_2 \longrightarrow [...] \longrightarrow HO^\bullet \quad (16)$$

$$WO_3(h^+) + IBP \longrightarrow INT \quad (17)$$

$$HO^\bullet + IBP \longrightarrow INT \quad (18)$$

$$WO_3(h^+) + INT \longrightarrow [...] \longrightarrow CO_2 + H_2O \quad (19)$$

$$HO^\bullet + INT \longrightarrow [...] \longrightarrow CO_2 + H_2O \quad (20)$$

Reaction (13) summarizes the direct IBP-O_3 steps that would lead to some large organic intermediates together with H_2O_2 detected and accumulated during single ozonation experiment, and eventually with the formation of $HO^\bullet$. On the other hand, visible light radiation provokes the creation of electron-hole pairs (reaction (14)) and electrons are proposed to react with dissolved O_3 and H_2O_2 through reactions (15) and (16), according to the profiles of these species during photocatalytic ozonation versus single ozonation. Finally, photogenerated holes and hydroxyl radicals can oxidize both IBP and any *INT* to achieve the complete mineralization into CO_2 and H_2O according to reactions (17)-(20).

The relative contribution of each step to the overall process would depend on the experimental conditions (e.g. pH, ozone dose or catalyst loading), and the confirmation of the intermediate species formed requires additional experimental work that will be the subject of a future work.

3.3. Catalysts screening for photocatalytic ozonation under visible-light radiation

All the catalysts prepared were tested in the photocatalytic ozonation of IBP under visible-light radiation. The results are depicted in **Fig.7** and **Fig.8** together with single ozonation results for the sake of comparison. Regarding the evolution of IBP (**Fig.7(A)**) results are quite similar although some trends can be extracted. First of all, slight differences were observed in the IBP adsorption capacity of the catalysts during the dark stage that is generally consistent with the values of pH_{PZC} obtained where a higher surface acid character led to a higher amount of initial IBP adsorbed. However, these differences seem not to play a crucial role in the behavior of the catalysts. On the other hand, it can be noticed that W-0 and W_{300}-1 catalysts gave place to similar IBP depletion rate than ozone alone whereas the rest of the catalysts gave place to a slight higher depletion rate. In general, the catalytic activity is increased as the heat-treatment (both in time and/or temperature) was increased. Main differences between ozone and O_3-photocatalytic processes were found in terms of mineralization (see **Fig.7(B))**. Ozone alone gave place to a 25% mineralization reached at about 60 min reaction time. On the other hand, the tungstite precursor, W-0, and the subsequent catalysts W_{300}-1 and W_{300}-3 showed a very different normalized TOC profile. It can be noticed a first step in which mineralization is slow, with a TOC removal rate fairly lower than during ozone alone reaction up to 60 min. After this time, the mineralization rate increased achieving around 35-40% of mineralization at 120 min with the three catalysts. It can be noticed that besides the differences in the properties of these three catalysts (E_g, S_{BET}, pH_{PZC}, etc.), they have in common that no monoclinic WO_3 crystallization has occurred during the heat-treatment applied. A significant increase of the catalytic activity is observed with the W_{300}-5 catalyst in terms of mineralization, reaching around 70% TOC removal at 120 min. The main differences of this and the previous catalysts are the presence of monoclinic crystalline phase to some extent in its structure according to XRD results. The best results were obtained with the 450ºC heat-treated catalysts reaching around 85-87% mineralization at 120 min reaction time. In these catalysts, an important contribution of monoclinic WO_3 higher than 75% was observed together with a higher pH_{PZC} which could indicate the presence of oxygen vacancies to some extent, although this could not be confirmed by XPS. The differences found in the mineralization profile of W_{450}-5 and W_{450}-30 catalysts, the first one leading to the highest mineralization rate, could be related to the higher S_{BET} found in this catalyst.

In addition, the evolution of dissolved ozone and hydrogen peroxide concentration formed during the reaction has been plotted in **Fig.8**. Regarding dissolved ozone (**Fig.8(A)**), it is noticeable the lower values of steady concentration with the most active catalysts, W_{450}-5 and W_{450}-30, compared to the single ozonation reaction. These results suggest an efficient O_3 consumption on the catalysts surface through its reaction with electrons generated in the photocatalytic process. **Fig.8(B)** shows the hydrogen peroxide concentration evolution with all the catalysts where the faster decomposition rate is also observed for the most active catalysts (W_{450}-5 and W_{450}-30), thus being likely indicative of a higher consumption of H_2O_2 in surface reactions as electron acceptor.

Therefore, at similar textural and optical properties, the monoclinic structure in WO_3 catalysts seems to be beneficial for the photocatalytic ozonation process with visible light.

3.4. Simulated solar light photocatalytic ozonation of ECs in MWW

The selected catalyst W_{450}-5 which presented the highest catalytic activity in the photocatalytic ozonation of IBP with visible light was tested in the photocatalytic ozonation of a mixture of ten ECs (AAP, MTP, CAF, HCT, ANT, SFM, CAR, KET, DCF and IBP) in a real municipal wastewater effluent. The characterization of the main parameters of the MWW effluent is summarized in **Table 2**. The photocatalytic ozonation treatment was carried out under the entire simulated solar light radiation from 300 nm. For comparative purposes also single ozonation treatment was carried out. The evolution of the ECs is depicted in **Fig.9**. It can be noticed that much of these compounds (AAP, ANT, SFM, CAR, KET and DCF) presented similar depletion rate both in single ozonation and photocatalytic ozonation treatments as a consequence of their high reactivity in O_3 direct reaction. Thus, the O_3 itself is highly effective to remove these compounds. Direct rate constants of ECs with O_3 are summarized in **Table S1**. On the other hand, the ECs whose rate constant is lower such as MTP, CAF, HCT and IBP, were faster eliminated through photocatalytic ozonation (in less than 60 min), being the differences found between ozone alone and the combined process higher as lower was the direct rate constant of O_3-EC reaction. Again in the MWW matrix main differences between ozone and photocatalytic ozonation were found in terms of TOC removal as shown in **Fig.10**. As it can be seen, ozone alone gave place to a lower degree of mineralization reaching less than 10% TOC removal after 120 min in contrast to a mineralization higher than 40% during photocatalytic ozonation. In addition, **Table 2** also shows the characterization of other important parameters in wastewater after the treatments being noticeable the decrease in COD and aromaticity when the combined treatment is applied. Finally, **Fig.11** shows the evolution of dissolved O_3 concentration together with the formation of H_2O_2 during the treatments. The obtained profiles are consistent with previous results thus indicating the consumption of both O_3 and H_2O_2 (formed through O_3-ECs direct reaction) at the WO_3 surface leading to the formation of additional oxidizing species such as hydroxyl radicals, which improve the mineralization reached. Thus, intermediate compounds formed from ECs oxidation are expected to be more easily eliminated through photocatalytic ozonation compared to single ozonation.

Therefore, the use of WO_3 as catalyst for photocatalytic ozonation of ECs containing MWW is an attractive alternative that improves the use of solar radiation leading to a fast elimination of organic contaminants (mainly those refractory to ozone reactions) and achieving an important mineralization degree.

4. Conclusions

WO_3 catalysts with different structural and surface properties where prepared by thermodecomposition of commercial tungstite ($H_2O{\cdot}WO_3$) at different temperatures, 300 and 450ºC, and short times, from 1 to 30 min. This heat-treatment allows obtaining tungstite, cubic and monoclinic crystalline phases of tungsten trioxide. In general, as time or temperature increased, monoclinic structure is formed which is also

accompanied by a reduction of specific surface area and an increase in the presence of oxygen vacancies. These properties, monoclinic structure together with the presence of oxygen vacancies played a key role in the behaviour of the WO_3 catalysts in the photocatalytic ozonation of IBP under visible light radiation, favouring the electron transport in the catalyst surface to some extent, thus improving the efficiency of the process. Among the treatments tested with the best catalytic system, photocatalytic ozonation showed a synergistic effect between ozone and irradiated WO_3 leading to a complete IBP depletion in less than 20 min with a degree of mineralization at about 87% at 120 min. Finally, the use of WO_3 as catalyst for photocatalytic ozonation of ECs in a MWW effluent with simulated solar radiation led to a fast elimination of the contaminants in less than 60 min and a mineralization degree higher than 40% at 120 min. The mechanism and kinetics of photocatalytic ozonation with WO_3 catalysts will be the subject of further work.

Acknowledgements

This work has been supported by the Spanish Ministerio de Economía y Competitividad (MINECO) and European Feder Funds through the project CTQ2012-35789-C02-01. Authors acknowledge the SACSS-SAIUEX and UAI-ICP for the characterization analyses. E. Mena thanks the Consejería de Empleo, Empresa e Innovación (Gobierno de Extremadura) and European Social Fund for providing her a predoctoral FPI grant (Ref. PD12059).

Appendix A. Supporting information

Supplementary data associated with this article can be found in the online version at XXXXXXXXX

References

Abe, R., Takami, H., Murakami, N., Ohtani, B., 2008. Pristine simple oxides as visible light driven photocatalysts: Highly efficient decomposition of organic compounds over platinum-loaded tungsten oxide. J. Am. Chem. Soc. 130, 7780–7781.

Agustina, T.E., Ang, H.M., Vareek, V.K., 2005. A review of synergistic effect of photocatalysis and ozonation on wastewater treatment. J. Photochem. Photobiol. C: Photochem. Rev. 6, 264–273.

Augugliaro, V., Litter, M., Palmisano, L., Soria, J., 2006. The combination of heterogeneous photocatalysis with chemical and physical operations: A tool for improving the photoprocess performance. J. Photochem. Photobiol. C Photochem. Rev. 7, 127–144.

Azimirad, R., Naseri, N., Akhavan, O., Moshfegh, A.Z., 2007. Hydrophilicity variation of WO3 thin films with annealing temperature. J. Phys. D: Appl. Phys. 40, 1134–1137.

Bader, H., Hoigné, J., 1981. Determination of ozone in water by the indigo method. Water Research 15, 449–456.

Barceló, D., Petrovic, M. (Eds.), 2008. Emerging contaminants from industrial and municipal wastes. Occurrence, analysis and effects. The Handbook of Environmental Chemistry 5-S1. Springer, Berlin (Germany).

Beltrán, F.J., 2004. Ozone reaction kinetics for water and wastewater systems. Boca Raton, CRC Press, Florida (USA).

Buffle, M., von Gunten, U., 2006. Phenols and amine induced HO· generation during the initial phase of natural water ozonation. Environ. Sci. Technol. 40, 3057–3063.

Cao, J., Luo, B., Lin, H., Xu, B., Chen, S., 2012. Thermodecomposition synthesis of WO3/H2WO4 heterostructures with enhanced visible light photocatalytic properties. Appl. Catal. B Environ. 111–112, 288–296.

Froment, G.F., Bishoff, K.B., 1979. Chemical Reactor Analysis and Design. John Willey & Sons. New York (USA).

González-Borrero, P.P., Sato, F., Medina, A.N., Baesso, M.L., Bento, A.C., Baldissera, G., Persson, C., Niklasson, G.A., Granqvist, C.G., Ferreira da Silva, A., 2010. Optical band-gap determination of nanostructured WO3 film. Appl. Phys. Letters 96, 061909-1–061909-3.

Guery, C., Choquet, C., Dujeancourt, F., Tarascon, J.M., Lassegues, J.C., 1997. Infrared and X-ray studies of hydrogen intercalation in different tungsten trioxides and tungsten trioxide hydrates. J. Solid Satate Electrochem. 1, 199–207.

Hernández-Alonso, M.D., Fresno, F., Suárez, S., Coronado, J.M., 2009. Development of alternative photocatalysts to TiO2: Challenges and opportunities. Energ. Environ. Sci. 2, 1231–1257.

Huber, M.M., Gobel, A., Joss, A., Hermann, N., Loffler, D., McArdell, C., Ried, A., Siegrist, H., Ternes, T.A., Von Gunten, U., 2005. Oxidation of pharmaceuticals during ozonation of municipal wastewaters effluents: A pilot study. Environ. Sci. Technol. 39, 4290–4299.

Johnson, P.N., Davis, R.A., 1996. Diffusivity of ozone in water. J. Chem. Eng. Data 41, 1485–1487.

Kanan, S.M., Lu, Z., Cox, J.K., Bernhardt, G., Tripp, C.P., 2002. Identification of surface sites on monoclinic WO3 powders by infrared spectroscopy. Langmuir 18, 1707–1712.

Lee, J.S., Jang, I.H., Park, N.G., 2012. Effects of oxidation state and crystallinity of tungsten oxide interlayer on photovoltaic property in bulk hetero-junction solar cell. J. Phys. Chem. C 116, 13480–13487.

Leitzke, A., Von Sonntag, C., 2009. Ozonolysis of unsaturated acids in aqueous solution: acrylic, methacrylic, maleic, fumaric and muconic acids. Ozone Sci. Eng. 31, 301–308.

Malato, S., Fernández-Ibáñez, P., Maldonado, M.I., Blanco, J., Gernjak, W., 2009. Decontamination and disinfection of water by solar photocatalysis: Recent overview and trends. *Catal. Today* 147, 1–59.

Mano, T., Nishimoto, S., Kameshima, Y., Miyake, M., 2011. Investigation of photocatalytic ozonation treatment of water over WO3 under visible light irradiation. J. Ceramic. Soc. Japan 119, 822–827.

Masschelein, W., Denis, M., Ledent, R., 1977. Spectrophotometric determination of residual hydrogen peroxide. Water Management. Water Sewage Works, August, 69–72.

Mena, E., Rey, A., Acedo, B., Beltrán, F.J., Malato, S., 2012. On ozone-photocatalysis synergism in black-light induced reactions: Oxidizing species production in photocatalytic ozonation versus heterogeneous photocatalysis. Chem. Eng. J. 204–206, 131–140.

Mvula, M., Von Sonntag, C., 2003. Ozonolysis of phenols in aqueous solution. Org. Biomol. Chem. 1, 1749–1756.

Nishimoto, S., Mano, T., Kameshima, Y., Miyake, M., 2010. Photocatalytic water treatment over WO3 under visible light irradiation combined with ozonation. Chem. Phys. Letters 500, 86–89.

Pang, H.F., Li, Z.J., Xiang, X., Fu, Y.Q., Placido, F., Zu, X.T., 2013. Hierarchical structured tungsten oxide nanocrystals via hydrothermal route: microstructure, formation mechanism and humidity sensing. Appl. Phys. A 112, 1033–1042.

Rakowski, S., Cherneva, D., 1990. Kinetics and mechanism of the reaction of ozone with aliphatic alcohols. Int. J. Chem. Kinetics 22, 321–329.

Santos, J.L., Aparicio, I., Callejón, M., Alonso, E., 2009. Occurrence of pharmaceutically active compounds during 1-year period in wastewaters from four wastewater treatment plants in Seville (Spain). J. Hazard. Mater. 164, 1509–1516.

Sein, M.M., Zedda, M., Tuerk, J., Schmidt, T.C., Golloch, A., Von Sonntag, C., 2008. Oxidation of diclofenac with ozone in aqueous solution. Environ. Sci. Technol. 42, 6656–6662.

Senthil, K., Yong, K., 2007. Growth and characterization of stoichiometric tungsten oxide nanorods by thermal evaporation and subsequent annealing. Nanotechnology 18, 395604-1–395604-7.

Subramanian, S., Noh, J.S., Schwarz, J.A., 1988. Determination of the point of zero-charge of composite oxides. J. Catal. 114, 433–439.

Sun, W.D., Zhao, Z.B., Guo, C., Ye, X.K., Wu, Y., 2000. Study of the alkylation of isobutene with n-butene over WO3/ZrO2 srong solid acid. 1. Effect of the preparation method, WO3 loading, and calcination temperature. Ind. Eng. Chem. Res. 39, 3717–3725.

Szilágyi, I.M., Fórizs, B., Rosseler, O., Szegedi, A., Németh, P., Király, P., Tárkányi, G., Vajna, B., Varga-Josepovits, K., László, K., Tóth, A.L., Baranyai, P., Leskelä, M., 2012. WO3 photocatalysts: Influence of structure and composition. J. Catal. 294, 119–127.

Tilley, R.J.D., 1995. The cristal chemistry of the higher tungsten oxides. Int. J. Refractory Metals Hard Mater. 13, 93–109.

Tomova, D., Iliev, V., Rakovsky, S., Anachkov, M., Eliyas, A., Li Puma, G., 2012. Photocatalytic oxidation of 2,4,6-trinitrotoluene in the presence of ozone under irradiation with UV and visible light. J. Photochem. Photobiol. A: Chem. 231, 1–8.

Tables and Figures captions

Table 1. Nomenclature, calcination conditions and some properties of the photocatalysts

Table 2. Characterization of MWW effluent

Figure 1. ATG-DTA profiles of H_2WO_4 precursor

Figure 2. XRD patterns of the catalysts

Figure 3. DR-UV-Vis spectra of the catalysts

Figure 4. (A) IBP and (B) TOC dimensionless concentration evolution during all the treatments applied with W_{450}-5 catalyst (lines show trends). Conditions: pH_0=6.5, T=25-35ºC, $C_{IBP,0}$=10 mg L^{-1}, C_{WO3}=0.25 g L^{-1}, $C_{O3ginlet}$=10 mg L^{-1}, Q_g=20 L h^{-1} (O_2 or O_3/O_2).

Figure 5. (A) Dissolved O_3 concentration and (B) H_2O_2 concentration during all the treatments applied with W_{450}-5 catalyst (lines show trends). Conditions: pH_0=6.5, T=25-35ºC, $C_{IBP,0}$=10 mg L^{-1}, C_{WO3}=0.25 g L^{-1}, $C_{O3ginlet}$=10 mg L^{-1}, Q_g=20 L h^{-1} (O_2 or O_3/O_2).

Figure 6. Experimental and simulated IBP dimensionless concentration evolution during single ozonation. Conditions: pH_0=6.5, T=25-35ºC, $C_{IBP,0}$=10 mg L^{-1}, $C_{O3ginlet}$=10 mg L^{-1}, Q_g=20 L h^{-1} (O_3/O_2).

Figure 7. (A) IBP and (B) TOC dimensionless concentration evolution during photocatalytic ozonation with all the catalysts studied (lines show trends). Conditions: pH_0=6.5, T=25-35ºC, $C_{IBP,0}$=10 mg L^{-1}, C_{WO3}=0.25 g L^{-1}, $C_{O3ginlet}$=10 mg L^{-1}, Q_g=20 L h^{-1} (O_3/O_2).

Figure 8. (A) Dissolved O_3 concentration and (B) H_2O_2 concentration during photocatalytic ozonation with all the catalysts studied (lines show trends). Conditions: pH_0=6.5, T=25-35ºC, $C_{IBP,0}$=10 mg L^{-1}, C_{WO3}=0.25 g L^{-1}, $C_{O3ginlet}$=10 mg L^{-1}, Q_g=20 L h^{-1} (O_3/O_2).

Figure 9. ECs dimensionless concentration during ozonation and photocatalytic ozonation with W_{450}-5 catalyst in a MWW effluent (lines show trends). Conditions: pH_0=6.5, T=25-35ºC, $C_{ECs,0}$=0.5 mg L^{-1}, C_{WO3}=0.25 g L^{-1}, $C_{O3ginlet}$=10 mg L^{-1}, Q_g=20 L h^{-1} (O_3/O_2).

Figure 10. TOC dimensionless concentration evolution during ozonation and photocatalytic ozonation with W_{450}-5 catalyst in a MWW effluent (lines show trends). Conditions: pH_0=6.5, T=25-35ºC, $C_{ECs,0}$=0.5 mg L^{-1}, C_{WO3}=0.25 g L^{-1}, $C_{O3ginlet}$=10 mg L^{-1}, Q_g=20 L h^{-1} (O_3/O_2).

Figure 11. (A) Dissolved O_3 concentration and (B) H_2O_2 concentration during ozonation and photocatalytic ozonation with W_{450}-5 catalyst in MWW effluent (lines show trends). Conditions: pH_0=6.5, T=25-35ºC, $C_{ECs,0}$=0.5 mg L^{-1}, C_{WO3}=0.25 g L^{-1}, $C_{O3ginlet}$=10 mg L^{-1}, Q_g=20 L h^{-1} (O_3/O_2).

Table 1. Nomenclature, calcination conditions and some properties of the photocatalysts

CATALYST	Calcination conditions	Tungstite (%)	Cubic (%)	Monoclinic (%)	S_{BET} ($m^2\ g^{-1}$)	pH_{PZC}	E_g (eV)
W-0	---	~100	0	0	27.8	4.71	2.42
W_{300}-1	300ºC, 1 min	82.0	18.0	0	28.7	4.39	2.43
W_{300}-3	300ºC, 3 min	0	100	0	40.3	4.13	2.64
W_{300}-5	300ºC, 5 min	0	85.7	14.3	39.0	4.18	2.65
W_{300}-60	300ºC, 60 min	0	80.3	19.7	n.m	n.m	n.m
W_{450}-5	450ºC, 5 min	0	23.9	76.1	30.2	5.25	2.65
W_{450}-30	450ºC, 30 min	0	9.5	90.5	21.1	4.98	2.67

n.m.: not measured

Table 2. Characterization of MWW effluent

PARAMETER	Before treatment	Ozonation	Photocatalytic ozonation
TOC (mgC L^{-1})	14.2	13.1	8.2
IC (mgC L^{-1})	0.19	0.15	0.20
Turbidity (NTU)	3.0	n.m.	n.m.
pH	6.5	5.9	5.7
Absorbance 254 nm	0.268	0.102	0.015
COD (mgO_2 L^{-1})	44	33	13
BOD (mgO_2 L^{-1})	28	n.m.	n.m.
Phosphate (mg L^{-1})	5	5	5

n.m.: not measured

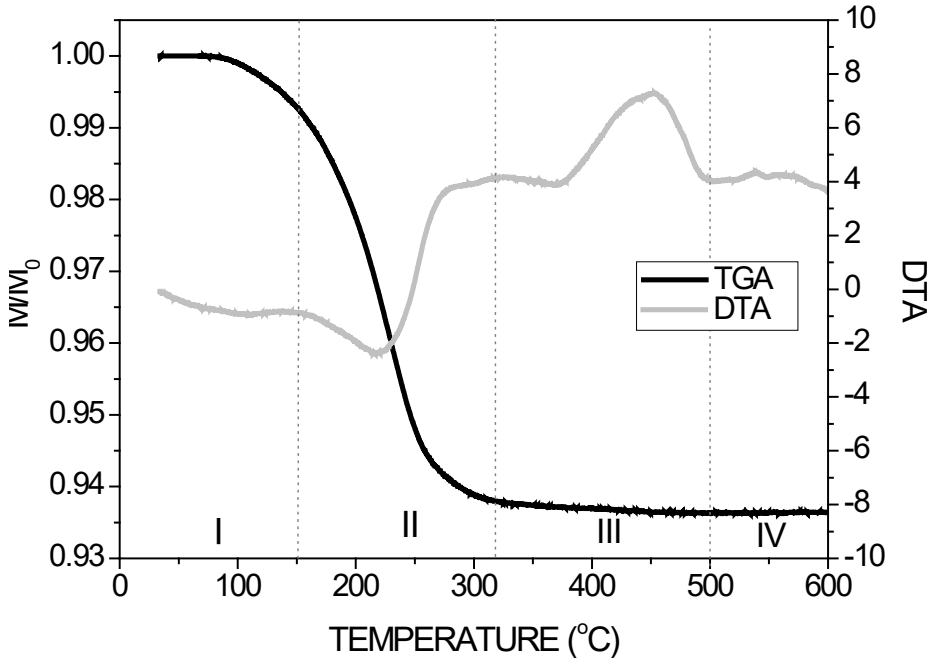

Figure 1. ATG-DTA profiles of H_2WO_4 precursor

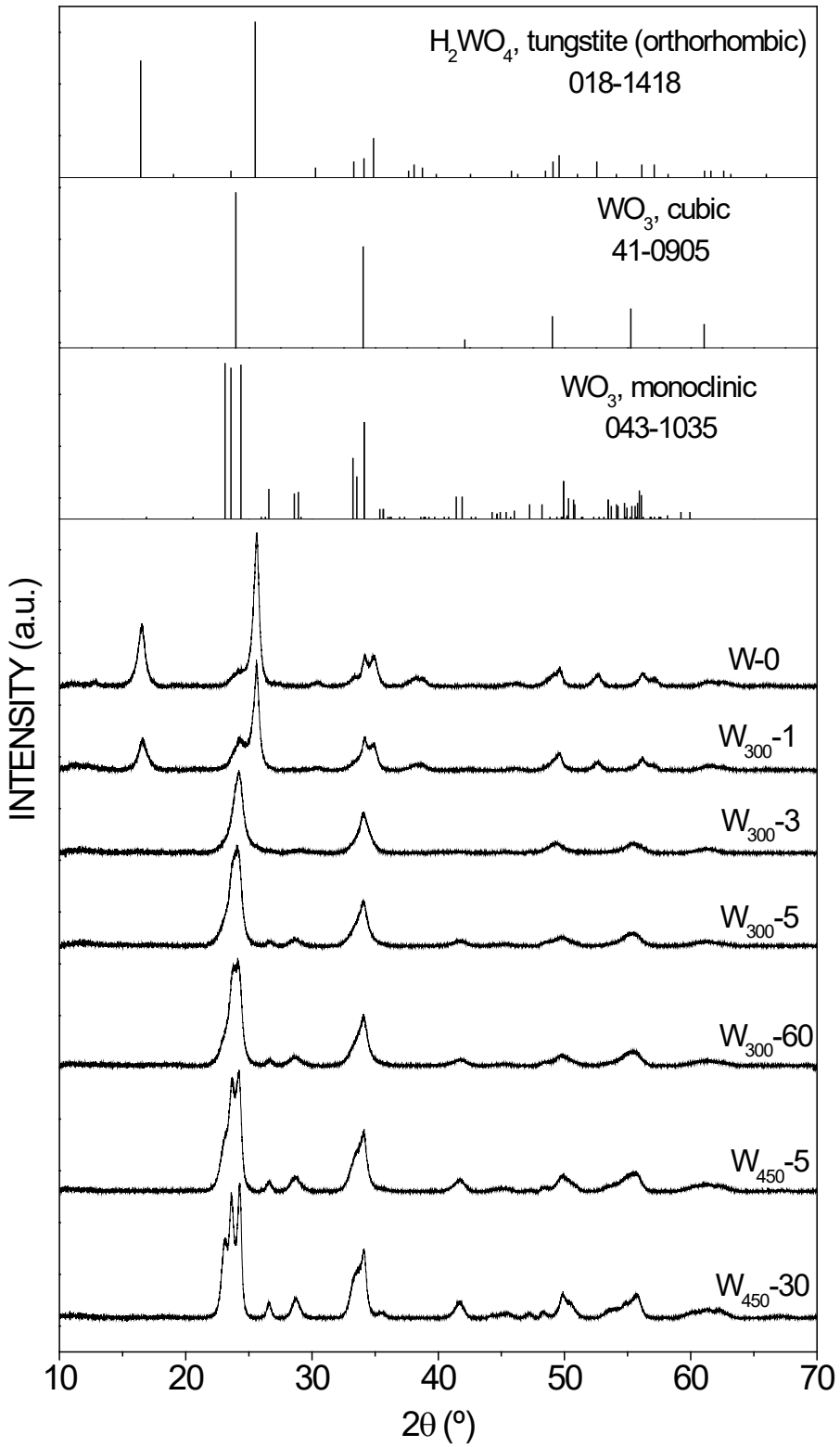

Figure 2. XRD patterns of the catalysts

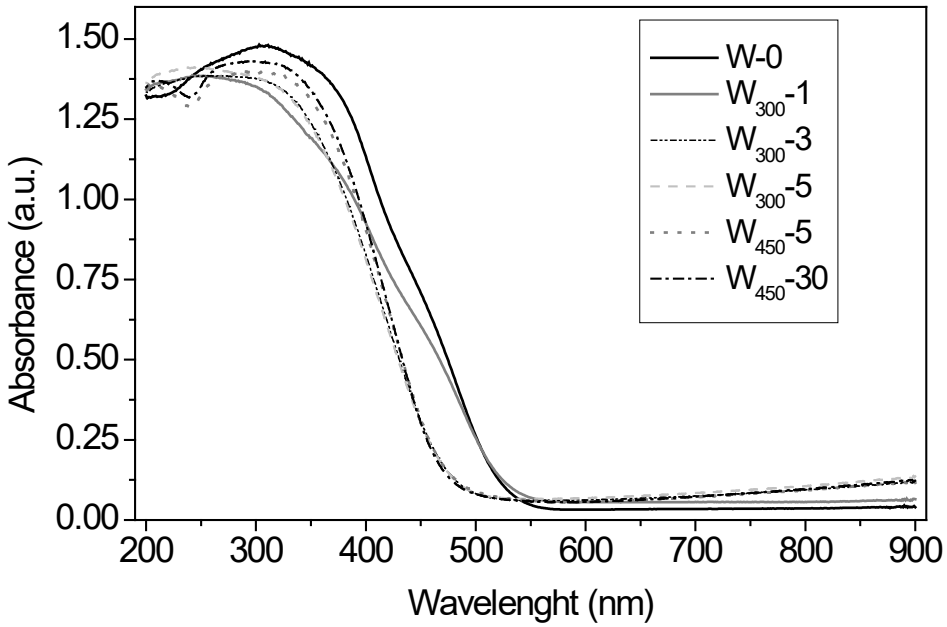

Figure 3. DR-UV-Vis spectra of the catalysts

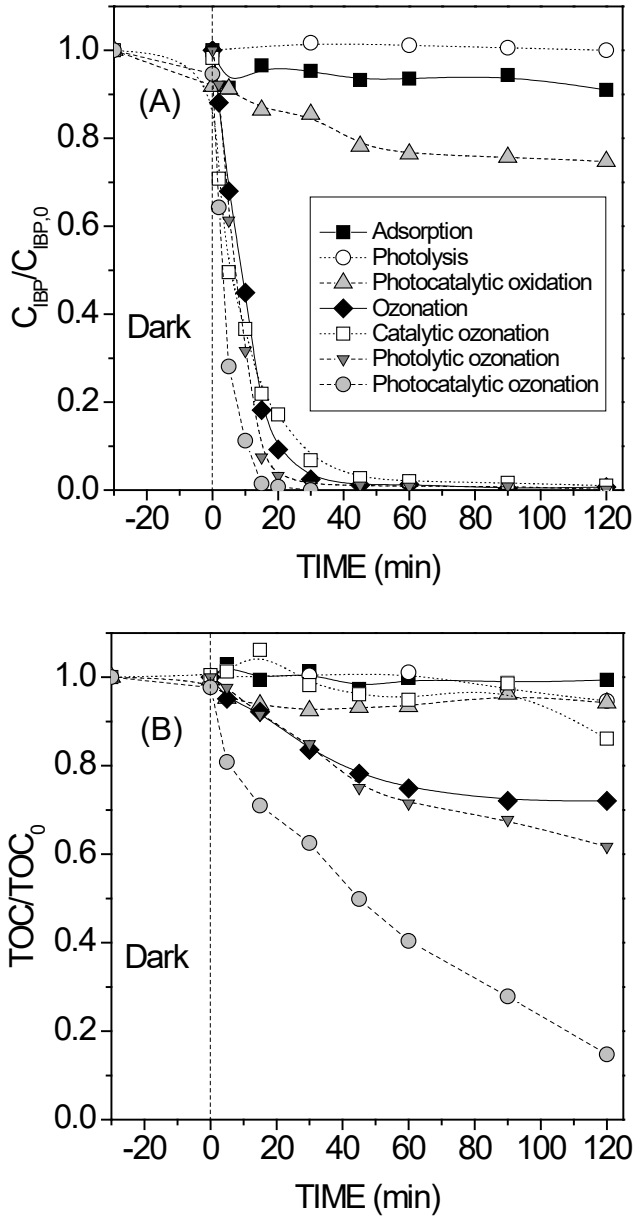

Figure 4. (A) IBP and (B) TOC dimensionless concentration evolution during all the treatments applied with W_{450}-5 catalyst (lines show trends). Conditions: pH_0=6.5, T=25-35ºC, $C_{IBP,0}$=10 mg L^{-1}, C_{WO3}=0.25 g L^{-1}, $C_{O3ginlet}$=10 mg L^{-1}, Q_g=20 L h^{-1} (O_2 or O_3/O_2).

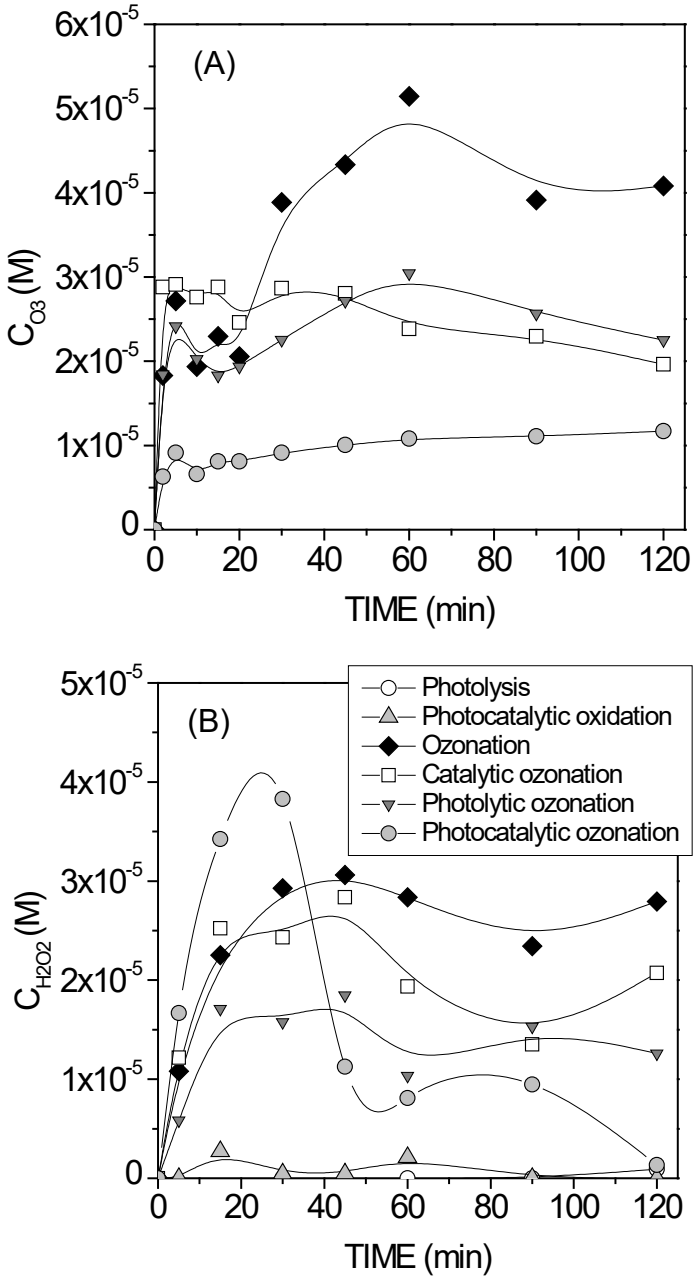

Figure 5. (A) Dissolved O_3 concentration and (B) H_2O_2 concentration during all the treatments applied with W_{450}-5 catalyst (lines show trends). Conditions: pH_0=6.5, T=25-35ºC, $C_{IBP,0}$=10 mg L^{-1}, C_{WO3}=0.25 g L^{-1}, $C_{O3ginlet}$=10 mg L^{-1}, Q_g=20 L h^{-1} (O_2 or O_3/O_2).

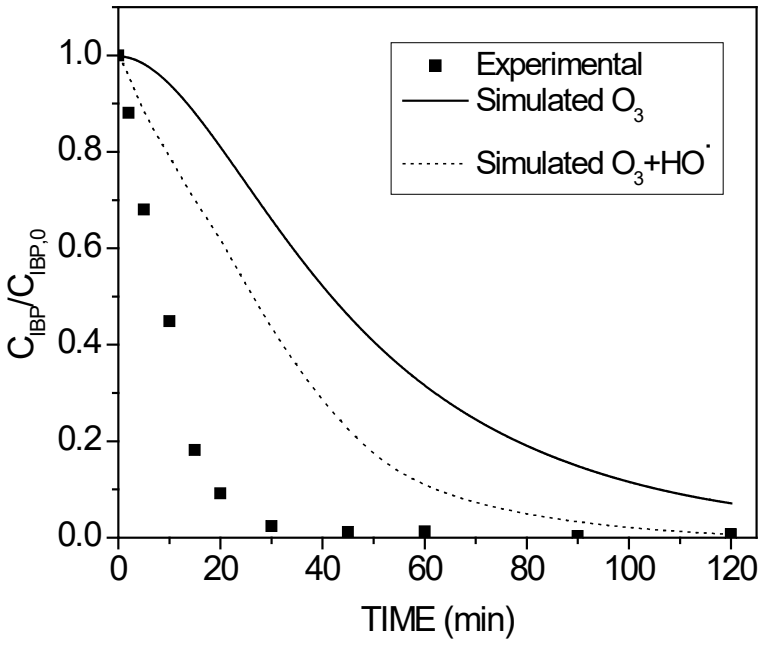

Figure 6. Experimental and simulated IBP dimensionless concentration evolution during single ozonation. Conditions: pH_0=6.5, T=25-35ºC, $C_{IBP,0}$=10 mg L^{-1}, $C_{O3ginlet}$=10 mg L^{-1}, Q_g=20 L h^{-1} (O_3/O_2).

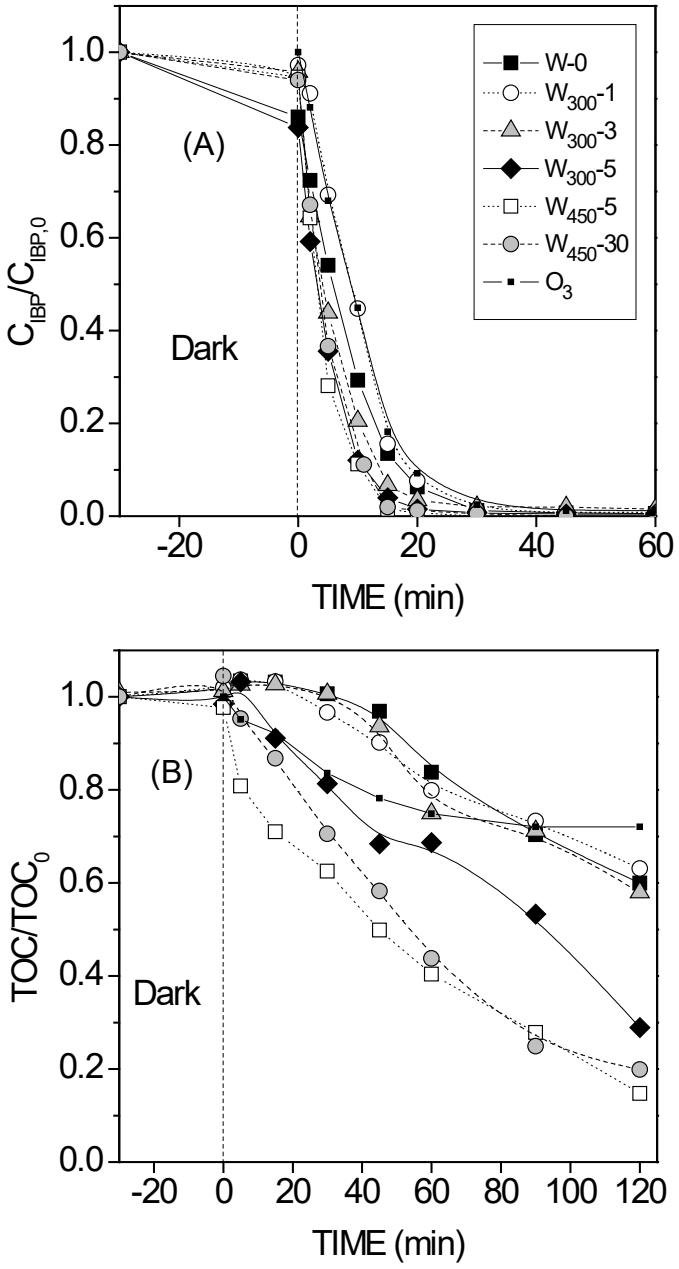

Figure 7. (A) IBP and (B) TOC dimensionless concentration evolution during photocatalytic ozonation with all the catalysts studied (lines show trends). Conditions: pH_0=6.5, T=25-35ºC, $C_{IBP,0}$=10 mg L^{-1}, C_{WO3}=0.25 g L^{-1}, $C_{O3ginlet}$=10 mg L^{-1}, Q_g=20 L h^{-1} (O_3/O_2).

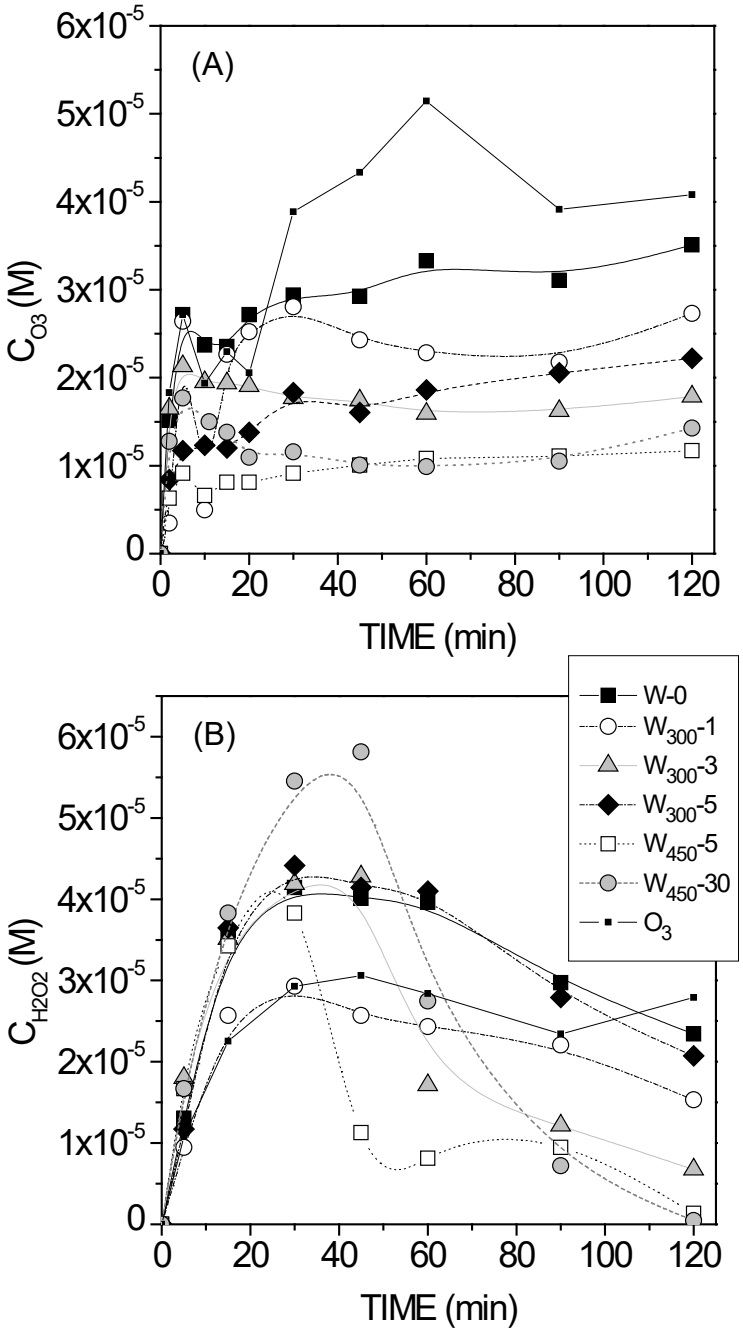

Figure 8. (A) Dissolved O_3 concentration and (B) H_2O_2 concentration during photocatalytic ozonation with all the catalysts studied (lines show trends). Conditions: pH_0=6.5, T=25-35ºC, $C_{IBP,0}$=10 mg L^{-1}, C_{WO3}=0.25 g L^{-1}, $C_{O3ginlet}$=10 mg L^{-1}, Q_g=20 L h^{-1} (O_3/O_2).

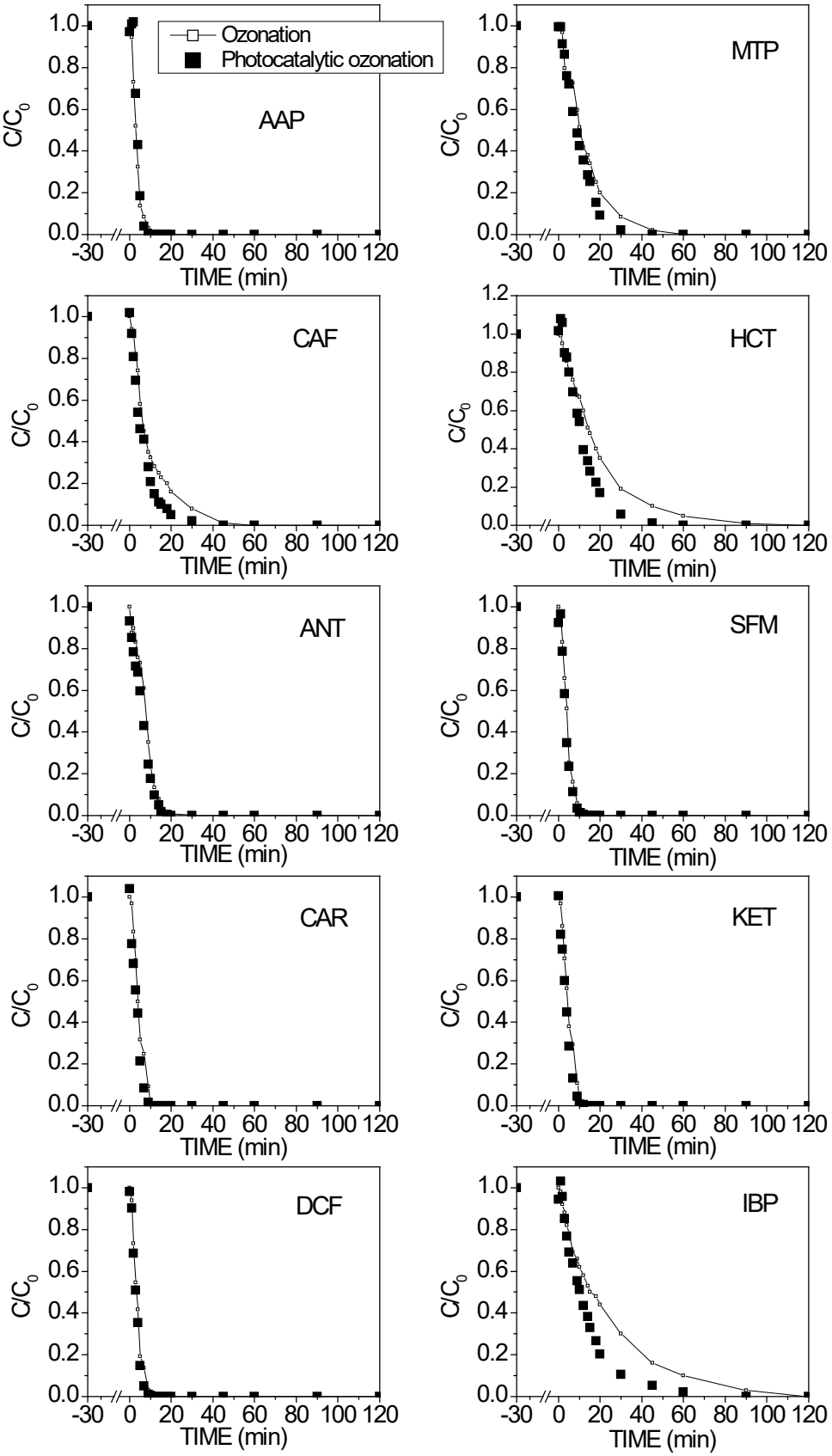

Figure 9. ECs dimensionless concentration during ozonation and photocatalytic ozonation with W_{450}-5 catalyst in a MWW effluent (lines show trends). Conditions: pH_0=6.5, T=25-35ºC, $C_{ECs,0}$=0.5 mg L^{-1}, C_{WO3}=0.25 g L^{-1}, $C_{O3ginlet}$=10 mg L^{-1}, Q_g=20 L h^{-1} (O_3/O_2).

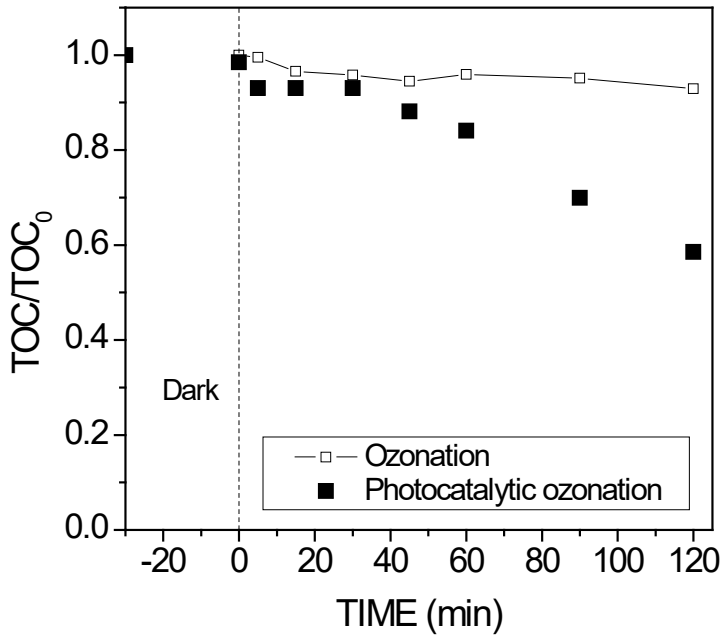

Figure 10. TOC dimensionless concentration evolution during ozonation and photocatalytic ozonation with W_{450}-5 catalyst in a MWW effluent (lines show trends). Conditions: pH_0=6.5, T=25-35ºC, $C_{ECs,0}$=0.5 mg L^{-1}, C_{WO3}=0.25 g L^{-1}, $C_{O3ginlet}$=10 mg L^{-1}, Q_g=20 L h^{-1} (O_3/O_2).

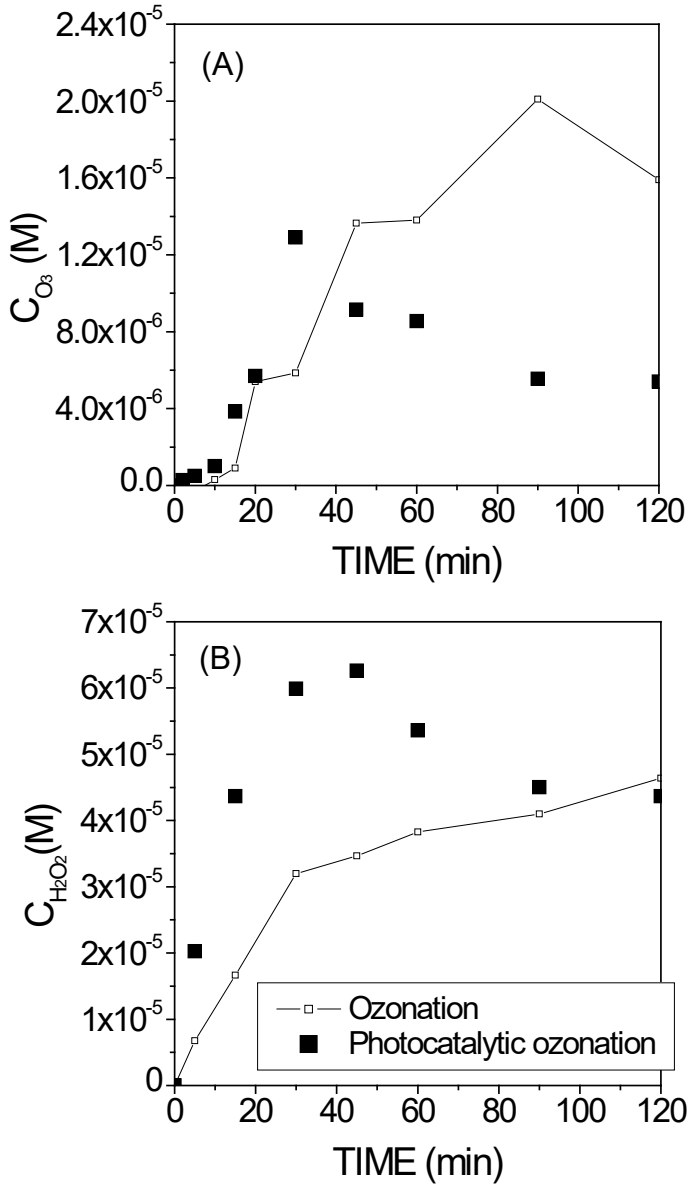

Figure 11. (A) Dissolved O_3 concentration and (B) H_2O_2 concentration during ozonation and photocatalytic ozonation with W_{450}-5 catalyst in MWW effluent (lines show trends). Conditions: pH_0=6.5, T=25-35ºC, $C_{ECs,0}$=0.5 mg L^{-1}, C_{WO3}=0.25 g L^{-1}, $C_{O3ginlet}$=10 mg L^{-1}, Q_g=20 L h^{-1} (O_3/O_2).